Environmental Science: Atmospheres

ROYAL SOCIETY OF CHEMISTRY

PAPER

View Article Online
View Journal | View Issue

Check for updates

Cite this: *Environ. Sci.: Atmos.*, 2022, **2**, 291

Particle emissions of a heavy-duty engine fueled with polyoxymethylene dimethyl ethers (OME)†

Alexander D. Gelner, *[a] Dieter Rothe,[b] Carsten Kykal,[c] Martin Irwin,[d] Alessandro Sommer,[a] Christian Pastoetter,[b] Martin Härtl,[a] Malte Jaensch[a] and Georg Wachtmeister[a]

Polyoxymethylene dimethyl ethers (OME) are promising substitutes for fossil diesel fuel. Besides the possibility of closing the carbon cycle, OME also feature soot-free combustion. Although this has been demonstrated sufficiently, nanoparticle emission in OME exhaust is mainly unknown. Many studies provide information about the particle size distribution (PSD) in the exhaust of OME-fueled diesel engines, but lack a distinction between solid particles and particles of a volatile nature. This distinction is necessary in order to evaluate the potential of OME regarding Euro VI and the Euro VII exhaust gas legislation being discussed. This study investigates the PSD of fossil diesel and the OME exhaust of a heavy-duty engine with and without removal of the volatile fraction *via* a catalytic stripper, by means of a purpose-built sampling system based on proposals from the Particle Measurement Programme (PMP). The experiments showed that most of the nuclei mode investigated in OME operation is of a volatile nature and that the solid particle number (PN) emission is below that of Euro VI diesel operation. Moreover, the results indicate that a state-of-the-art aftertreatment system removes most of the particle emission, regardless of whether it is volatile or solid. Selective catalytic reduction using aqueous urea dosing increases solid particle emission, especially in the sub-23 nm range. However, a PMP-conformant measurement of PN_{23} and PN_{10} during WHSC and WHTC runs demonstrated that the PN emission of an OME-fueled engine falls below the average immission level of urban and regional background in Germany.

Received 19th October 2021
Accepted 3rd January 2022

DOI: 10.1039/d1ea00084e

rsc.li/esatmospheres

Open Access Article. Published on 15 febbraio 2022. Downloaded on 01/08/2025 15:13:15.
This article is licensed under a Creative Commons Attribution 3.0 Unported Licence.

Environmental significance

OME as sustainable e-fuel helps to reduce the impact of diesel engines on the environment regarding climate change and air pollution due to black carbon emission. Although the soot-free combustion of OME is well demonstrated, the emission of nanoparticles in the exhaust of an OME-fueled engine has been poorly characterized. This study investigates the particle size distribution of OME exhaust with respect to good practices in aerosol measurement technology. The results help to evaluate the environmental impact of OME-fueled compression ignition engines and demonstrate the importance of exhaust measurement standards regarding sampling systems for particle measurement.

Introduction

It is widely accepted that in order to better mitigate climate change, anthropogenic greenhouse gas emissions must be reduced, primarily carbon dioxide (CO_2).[1] Although there has been a push for mobile applications used to migrate to battery-electric vehicles operated with renewable power, substituting fossil fuels with renewable, synthetic, electricity-based fuels is a beneficial short-term and target-oriented approach that can be performed with relative ease alongside the move towards electrification. These so-called e-fuels offer the possibility of diminishing the CO_2 impact of existing and future internal combustion engines; the present fuel distribution infrastructure can mostly be used.[2] In the case of diesel engines, long-chain polyoxymethylene dimethyl ethers (OME) have physico-chemical properties similar to that of fossil diesel and are among the most promising of e-fuels.[3] The synthesis process of renewable OME-fuel over formaldehyde and methanol starts with hydrogen and CO_2,[4] hence offering the potential for a closed carbon cycle. The prerequisite for this process is hydrogen from renewable sources, such as electrolysis by solar or wind power. Furthermore, CO_2 must be obtained by post-combustion capture or direct air capture,[5] and the synthesis process must not lead to additional CO_2 emissions. In addition to the possibility of renewable production, OME also provides

[a]*Technical University of Munich (TUM), Schragenhofstraße 31, 80992 Munich, Germany. E-mail: gelner@tum.de*

[b]*MAN Truck & Bus SE, Vogelweiherstraße 33, Nuremberg, Germany*

[c]*TSI GmbH, Neuköllner Straße 4, 52068 Aachen, Germany*

[d]*Catalytic Instruments GmbH & Co. KG, Zellerhornstraße 7, 83026 Rosenheim, Germany*

† Electronic supplementary information (ESI) available. See DOI: 10.1039/d1ea00084e

© 2022 The Author(s). Published by the Royal Society of Chemistry

Open Access Article. Published on 15 febbraio 2022. Downloaded on 01/08/2025 15:13:15.
This article is licensed under a Creative Commons Attribution 3.0 Unported Licence.

the advantage of soot-free combustion.[6–10] The reason for this is the intramolecular lack of C–C-bonds, which suppresses the formation of soot precursors such as polyaromatic hydrocarbons.[11] This resolves the trade-off between soot and nitrogen oxide (NO_x) emissions from diesel engines[6] and opens up the opportunity for massive NO_x reduction in the raw exhaust by measures such as high exhaust gas recirculation (EGR) rates or decreased injection pressure.[12,13] Soot and nitrogen oxide emissions are both harmful to the human body[14,15] and the environment.[16,17] Therefore, the resolution of this trade-off supports the efforts for air pollution control being implemented by governmental regulations of emission legislation.

However, although many studies have demonstrated the soot-free combustion of OMEs, the extent of nanoparticle emissions in the exhaust has been poorly characterized. According to Kittelson, particles form a trimodal size distribution in the exhaust of a diesel engine.[18] The nuclei mode with particles of electrical mobility diameter from typically 5 to 50 nm consists of mostly volatile organic and sulfur compounds formed during exhaust dilution and cooling, as well as solid carbon and metal compounds. The accumulation mode with particles between 100 nm and 300 nm contains carbonaceous agglomerates and associated adsorbed materials and makes up most of the particle mass. The coarse mode consists of accumulation mode particles, which re-entrain to the exhaust after growth during deposition on surfaces in the exhaust system. The current legislation considers only solid particles with a diameter of 23 nm and larger, although future legislative proposals are pushing this to <23 nm with a 10 nm-cut-point.[19,20] The Particle Measurement Programme (PMP) by UN/ECE recommends the removal of volatile particles by means of evaporation or catalytic conversion.[21] Although many studies have examined this topic, the composition of the particle size distribution (PSD) in OME exhaust remains unknown. Lin *et al.* and Liu *et al.* studied the PSD of diesel exhaust and blends with OME up to a volumetric mixing ratio of 30% and varying different effects on the accumulation mode, depending on the injection pressure[22] and the operating point.[23] Ferraro *et al.* investigated the effect of OME_3 on soot particle formation in a premixed ethylene burner and observed a shift of the maxima towards smaller particle diameters.[24] Popp *et al.* also observed this effect with OME-diesel-blends on a heavy-duty engine.[25] Investigations with an OME_{3-5} mix in a single-cylinder research engine demonstrated particle emissions in the so-called sub-23 nm range with a peak around a size of 10 nm.[26,27] Neither study included a description of the sampling system, so it is unknown whether or not the results contained volatile particles. Preuß *et al.* observed an increase of this sub-23 nm mode with increasing mixing ratios of OME_{3-5} in blends with hydrogenated vegetable oil (HVO) and rapeseed methyl ester used as diesel reference fuels, but also without specifying the sampling system.[28] Barro *et al.* observed a similar peak in OME exhaust, located at the nuclei mode of diesel exhaust.[29] An additional investigation in that study using transmission electron microscopy (TEM) indicated that some of the observed particles below 20 nm consisted of soot and metal particles. They therefore assumed that the measured particles in this range were solid in nature, although the particle measurement device did not include a volatile particle remover. Dworschak *et al.* compared the PSD of neat OME_3, OME_4 and OME_5 [30] as well as a mix of OME_{2-6} [31] to the PSD of HVO as a diesel reference fuel. The sampling system used in these studies contained an evaporation tube for volatile particle removal. Neither of these studies had results demonstrating a particle emission peak around 10 nm. In order to distinguish between volatile and solid particles in the PSD of OME, a systematic observation within the scope of the present work investigated the exhaust of a state-of-the-art heavy-duty engine with a modular exhaust aftertreatment system (ATS), by means of several sampling systems, which differ in dilution. The systems for solid particle measurement only, contain a catalytic stripper for the removal of volatile particles according to Abdul-Khalek & Kittelson[32] and Swanson & Kittelson.[33] A two-stage dilution sampling system enables a comparison of the PSD in raw exhaust in diesel and OME operation. Removing the second dilution stage makes the investigation of the volatile and nonvolatile PSD of OME more accurate and enables an investigation of the difference between raw exhaust and tailpipe particle emissions. Moreover, this work contains an investigation on the effect of urea dosing on the particle emissions of an OME engine with a twin-dosing system for selective catalytic reduction (SCR). Another series of experiments indicates the effect of a diesel particulate filter (DPF) and urea dosing on the solid particle number (PN) emission in the legislative test cycles "World harmonised steady-state cycle" (WHSC) and "World harmonised transient cycle" (WHTC) with a PMP-conform exhaust measurement and an additional sampling of sub-23 nm particles. An outlook evaluates the potential of OME as a carbon-neutral and low-emission alternative diesel fuel.

Materials and methods

Tested fuels

Polyoxymethylene dimethyl ethers (OME) are oligomers from the group of C_1 oxygenates. They have the chemical structure of CH_3–O–$(CH_2O)_n$–CH_3, while n as the number of oxymethylene groups is often used as an index to specify the respective OME_n. In this work, the abbreviation OME refers to a mixture with major percentages of $n = 3$–6 (OME_3: 58%, OME_4: 29%, OME_5: 10%, OME_6: 2%), which fulfills the M DIN TS 51699 standard for OME-fuel.[34] The mixture also contains 300 mg kg^{-1} each of butylated hydroxytoluene (BHT) for oxidation stabilization, and a flow improver as additives. Fossil diesel according to the EN 590 standard with a maximum content of 7% (v/v) fatty acid methyl esters (FAME) sets the reference fuel for comparing the particle emission behavior. ASG Analytik-Service AG provided the OME-fuel and determined the values of the physical properties. The ESI† contains the respective standard of the measurement method used for providing the substance values. Table 1 compares these values with the EN 590 standard. The oxygen content of OME is around 45% (w/w). This reduces the lower heating value (LHV) of the fuel to about 2.2 times lower than that of fossil diesel. The higher density of OME compensates this marginally, resulting in a volumetric diesel equivalent

 © 2022 The Author(s). Published by the Royal Society of Chemistry

Open Access Article. Published on 15 febbraio 2022. Downloaded on 01/08/2025 15:13:15.
This article is licensed under a Creative Commons Attribution 3.0 Unported Licence.

Table 1 Properties of the tested fuels. ASG Analytik-Service AG determined the values of OME; the values of diesel come from Lautenschütz *et al.*[36] if not specified in the standard EN 590.[35] The calculation of the gravimetric oxygen content of diesel is based on the values from Hoekman *et al.*,[37] with the assumption that the FAME proportion is made of oleic acid

	Diesel	OME
Cetane number	>51	69
Lower heating value in MJ kg^{-1}	42.6 [36]	19.2
Oxygen content in % (w/w)	0–1 [37] (with max. 7% (v/v) FAME)	45
Density in kg m^{-3}	820–845	1057
Boiling range in °C	170–390 [36]	145–242
Flash point in °C	>55	65
Sulfur content in ppm	<10	<5

ratio of around 1.7 liters of OME for 1 liter of diesel. The flash point of the OME mixture investigated exceeds the requirements of the EN 590 standard,[35] which enables storage and distribution systems similar to fossil diesel. Values of the boiling range of diesel come from Lautenschütz *et al.*,[36] who have determined characteristic values of diesel according to EN 590. The calculation of the volumetric diesel equivalent ratio also uses the LHV of diesel from this publication. The sulfur content of OME is lower than 5 ppm according to DIN EN ISO 20884:2011, so it reaches the lower limit of the determination standard for this value. Because of the sulfur-free educts and synthesis of OME, the sulfur content is furthermore assumed to be less than 1 ppm.

Test engine and operating points

The test engine used was a MAN D2676LF51 six-cylinder heavy-duty diesel. Apart from the high-pressure fuel pump seals, the engine was not specially adapted for OME operation. Therefore, the engine components, such as the piston geometry and cylinder head, were optimized for operation with conventional fossil diesel. In order to avoid long and inefficient combustion durations due to the lower-level heating value,[38] the solenoid injectors for OME operation had higher nozzle flow rates. Besides the effect of decreasing efficiency during longer combustion durations, interactions of the fuel jet with the lubricant oil film are undesirable. Therefore, higher nozzle flow rates enabled a shorter injection process which stops before the piston reveals the liner during the downward movement. The ESI† displays the properties of the test engine.

The test engine had a modular aftertreatment system provided by VT Vitesco Technologies Emitec GmbH, which enabled removal or exchange of the components. The system had a twin-dosing design, which means that there were two positions, in which urea dosers provide the reducing agent for the selective catalytic reduction in the form of aqueous urea solution according to ISO 22241-1:2019, abbreviated as AdBlue®.[39] The injection and conversion of the aqueous urea solution to ammonia (NH_3) happens in a so-called Universal Decomposition Pipe (UDP) equipped with a titanium dioxide (TiO_2)-coated hydrolysis catalyst (Hyd).[40] The copper-zeolite (CuZe) SCR catalysts reduce NO_x with the reducing agent NH_3.[41] An ammonia slip catalyst (ASC) oxidizes excess ammonia after the SCR system selectively in order to avoid an unselective oxidation to nitrous oxide (N_2O) in the diesel oxidation catalyst (DOC) placed downstream.[42] The DPF was an uncoated Cordierite wall flow filter. A second SCR stage ideally converted any remaining NO_x emissions. The second stage had no ASC installed. The ESI† displays the properties of the ATS components.

The investigation of the PSD focused on two stationary operating points: L1 represents a high-load point with comparatively high exhaust gas temperatures; L2 represents a low-load point with high engine speed, resulting in lower exhaust gas temperatures and higher space velocities than L1. Table 2 describes the parameter settings of the operating points in diesel and OME operation.

Measuring setup

The Scanning Mobility Particle Sizer (SMPS, TSI Model 3938) ascertained the PSD in the exhaust gas and contained the following components: the model 3082 classifier selected the exhaust gas by electrical mobility classification into a monodisperse aerosol *via* the following steps: a Model 3088 soft X-ray neutralizer ionized the aerosol carrier gas, leading to a bipolar charge distribution.[43] The model 3081A differential mobility analyzer (abbreviated as "longDMA") selected particles in the aerosol according to their electrical mobility diameter. The ultrafine condensation particle counter (TSI Model 3776, with a 50% cut-off at 2.5 nm) determined the particle number of the respective particle size range. Upstream of the aerosol inlet of the classifier, an impactor separated large particles above the set SMPS measurement range in order to minimize the deviation of the multiple charge correction[44] in the TSI "Aerosol Instrument Manager" evaluation software. The measurement range of the SMPS in this work was set to 6.38 nm to 224.7 nm. The sampling duration of every run was 72 seconds, including the automatic purging process of the SMPS.

The equipment for particle number measurements during the test cycles consisted of an AVL Advanced Particle Counter 489, standard equipped with a condensation particle counter (CPC) with a 50% cut-off at 23 nm. This measurement device fulfilled the specifications of PMP.[21] It contained a PN_{23}-compliant volatile particle remover (VPR), consisting of three elements according to the PMP in this chronological order: a hot dilution with a minimum dilution ratio of one to ten stabilized the aerosol and reduced the particle concentration;

Open Access Article. Published on 15 febbraio 2022. Downloaded on 01/08/2025 15:13:15.
This article is licensed under a Creative Commons Attribution 3.0 Unported Licence.

Table 2 Operating points for measurement of the PSD. The pressure indication system AVL Indimodul 621 and an optical encoder determined the respective point in time with 50% mass fraction burnt (MFB50) in degrees of crank angle (CA) after the top dead center (TDC). The engine's lambda probe determined the air–fuel-ratio (λ)

	Diesel		OME	
Load point	L1	L2	L1	L2
Engine speed in RPM	1100	2000	1100	2000
Brake mean effective pressure in bar	18	6	18	6
Rail pressure in bar	1200	1800	1000	1600
MFB50 in °C after TDC	9	6	15	6
EGR rate in % (w/w)	20	33	18	43
Air-fuel ratio λ	1.35	2.30	1.45	1.90
Exhaust temperature downstream of the second turbocharger in °C	410	260	370	250

an evaporation tube heated to 350 ± 50 °C vaporized volatile material like the condensed fuel drops mentioned by Kittelson;[18] a cool dilution with a minimum dilution ratio of one to ten decreased the temperature of the aerosol and reduced the particle concentration and avoided re-nucleation of the evaporated substances. Furthermore, an additional CPC with a 50% cut-off at 10 nm (TSI Model 3772, calibrated by the Federal Institute of Metrology METAS), connected with the secondary outlet of the APC, enabled a synchronous PN measurement, including the sub-23 nm range. In this additional measurement setup, an auxiliary pump enabled a flow rate of 1.0 l min^{-1} through the CPC, controlled by an internal critical orifice.

While the APC had an integrated sampling system which was connectable to the respective location at the exhaust pipe, the measurement setup for PSD determination with the SMPS required a purpose-built sampling system. In this work, this sampling system contained the following elements, which were based on the PMP proposals: the exhaust gas flowed through an ejector diluter (DEKATI diluter with a dilution ratio of one to ten). A heating cover with a set temperature of 200 °C reduced the cooling of the aerosol. In addition, the filtered and dried dilution air flowed through a heater set to 150 °C. A "Catalytic Stripper CS10" (hereinafter abbreviated as CS) according to Abdul-Khalek & Kittelson[32] and Swanson & Kittelson,[33] provided by Catalytic Instruments GmbH & Co. KG enabled removal of volatile particles with an operational set temperature of 350 °C. The operational performance of the CS is well documented in the literature.[45–52] A diluted aerosol flow enters the device whose temperature is elevated to the operational setpoint of 350 °C. The aerosol flow then enters the catalyst monolith, where, in the presence of oxygen, hydrocarbon (HC) particles evaporate and HC vapors are converted into the gaseous water (H_2O) and CO_2. The residence time within the monolith is a function of the flow rate and the design value chosen to balance between HC conversion efficiency and particle penetration. The CS is optimized for this balance, ensuring that even the most stringent legislative tests pose no problem for the performance of this device. Some sulfur present in the aerosol is adsorbed to the catalyst itself, which directly acts as a sulfur trap, minimizing artifacts caused by sulfuric acid.[33] If high-sulfur fuels are used, then the CS requires servicing, but this was not the case for these experiments. The CS also oxidizes organic substances adhering to solid particle cores, which suppresses an increase in the size of the particles due to this phenomenon.[18] It is possible to directly compare solid and non-solid fractions of aerosol in the sampling system by alternating the use of the CS. Sampling without the CS results in a "total particle" concentration, and with the CS the "solid particle concentration". Subtracting the solid from the total gives an approximation of the volatile fraction. An integrated cooler inside the CS resulted in an outlet temperature of approximately 30 °C. In order to avoid overwhelming the measurement equipment by exceedingly high particle concentrations, a second ejector diluter (DEKATI Diluter with a dilution ratio of one to eight) reduced the particle concentration downstream of the CS. Due to the integrated cooler inside the CS, the cooling function of this dilution was obsolete in the setup with the CS. The removal of this second dilution stage enabled a higher measurement accuracy due to a higher particle concentration upstream of the measurement device in an operation with a lower level of particle emission. The CPC connected to the SMPS system had a flow rate of 1.5 l min^{-1}. The "Catalytic Stripper CS10" is designed for a nominal aerosol flow of 10 standard liter per minute (SLPM). In order to use the device at this flow, an auxiliary vacuum pump connected with a tee at the inlet of the SMPS increased the total flow in the sampling system to the respective nominal flow of the CS. The tubing to the auxiliary pump used the specific connection to the tee, which had an offset of 90° to the aerosol flow from the sampling system towards the impactor of the SMPS. Fig. 1 depicts a scheme of the sampling systems for the determination of the PSD using the SMPS and the PN emission in the test cycles using the AVL APC.

The purpose-built sampling system requires calculating the respective particle concentration reduction factor (PCRF) due to transport losses depending on the particle size. Von der Weiden *et al.* developed a "Particle Loss Calculator"[53] according to mechanisms described by Hinds[54] and Willeke & Baron.[55] Although the estimation of the transport losses in this work did not use this specific calculator, it was based on the mechanisms mentioned in ref. 53. The calculation of losses due to gravitational settling in the inlet, sedimentation, bent tubing and coagulation[55] resulted in a transportation efficiency of more than 99.9% for a minimal particle diameter of 6 nm and a maximal particle diameter of 0.23 μm. They are therefore

 © 2022 The Author(s). Published by the Royal Society of Chemistry

Open Access Article. Published on 15 febbraio 2022. Downloaded on 01/08/2025 15:13:15.
This article is licensed under a Creative Commons Attribution 3.0 Unported Licence.

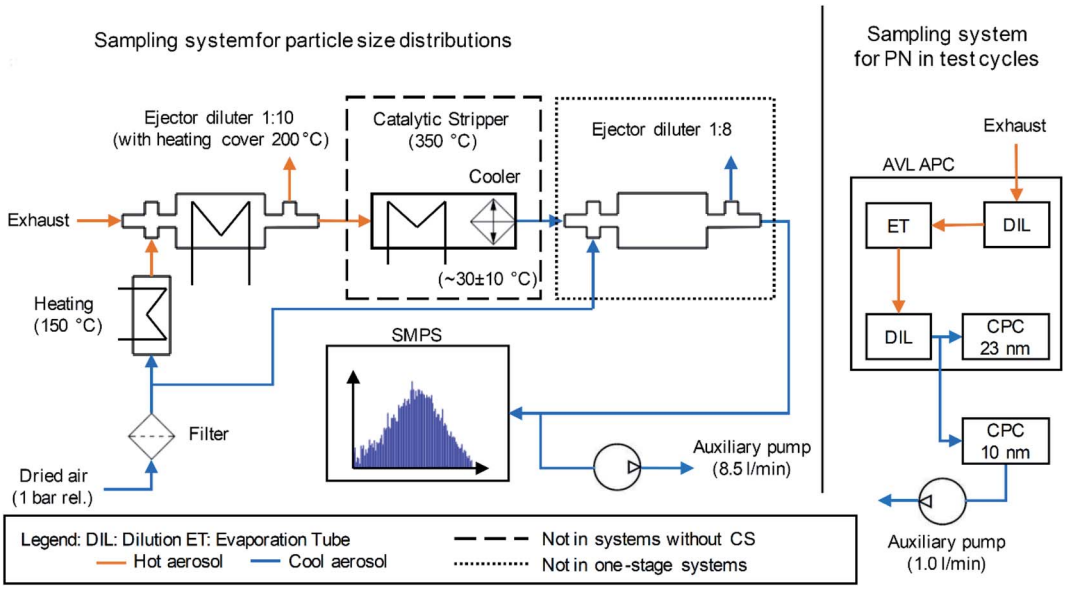

Fig. 1 Scheme of the sampling systems.

neglected in the following. This is due to the isokinetic sampling, the tube inner diameter of 6 mm and the mean flow velocity of approximately 5.9 m s^{-1}. The Reynolds number inside the tubing was about 2350, which allows an estimation of a laminar flow. Thermophoretic losses according to ref. 54–56 were neglected except for the CS, because the calculation of the thermophoretic velocity results in less than 0.001 m s^{-1} for the sampling system in this work. Moreover, transport losses due to electrostatic fields were neglected due to the usage of stainless steel wherever possible and an intermediate connection using Tygon tubing. This polymer is known as a tubing material having lower electrostatic losses than other kinds of tubing.[57–59] However, the manufacturer of the catalytic stripper (Catalytic Instruments GmbH & Co. KG) provides in the manual, penetration efficiency data at nominal flow (10 l min^{-1}) due to diffusional and thermophoretic losses. The loss calculation uses this penetration efficiency, supplemented by a calculation of the transportation losses due to Brownian diffusion according to Hinds.[54] Additionally, the transportation losses of the ejector diluters were assumed to be 5% for each diluter and for any particle diameter, according to the measurements of Giechaskiel *et al.*[60] Fig. 2 shows the calculated penetration efficiencies of the purpose-built sampling systems with and without the CS or the second dilution stage. The ESI† shows a detailed calculation of the mentioned losses. The results of the PSD in this work use the PCRF of these calculations. Furthermore, the TSI "Aerosol Instrument Manager" software includes the option of considering the diffusion losses inside the SMPS and a multiple charge correction. The evaluations in this study include these considerations.

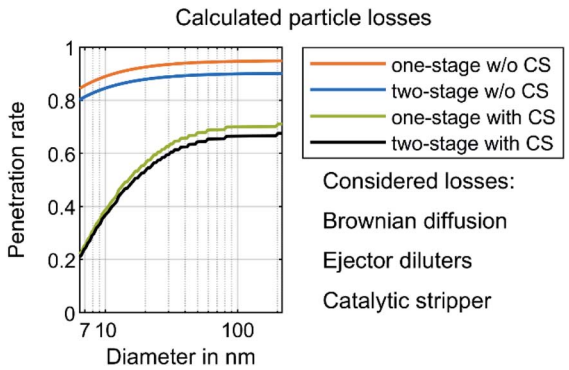

Fig. 2 Calculated particle losses. The losses due to Brownian diffusion are based on calculations according to Hinds[54] with the assumption of a laminar flow inside the tubing. The losses of each ejector diluter were assumed to be 5% according to Giechaskiel *et al.*[60] The manufacturer of the catalytic stripper determined the respective penetration efficiency at a nominal flow rate of 10 l min^{-1}.

Since the setup for PN measurement contained a commercial device in the form of the AVL APC 489, the manufacturer specifies a respective value of the PCRF in this setup. The evaluation in this study uses this PCRF for the correction of the particle number emission determined by the CPCs during the test cycles. Particle losses in the Tygon tubing from the secondary outlet to the CPC with a 50% cut-off at 10 nm were disregarded due to a tubing length of 300 mm, resulting in an overall penetration rate of more than 95% for particles with a diameter larger than 10 nm regarding the losses considered in the purpose-built sampling system.

Test procedure

The ESI† shows the chronological order of the experiments for measuring the PSD on the stationary operating points presented in Table 2. In order to avoid artifacts in the form of adsorbed organic substances during the operation without the CS, the test run with the consideration of volatile particles took place after the test run using the CS. After the operation without the CS, a cleaning procedure using the CS and the auxiliary pump with a duration of 60 minutes for the removal of adhering

Open Access Article. Published on 15 febbraio 2022. Downloaded on 01/08/2025 15:13:15.
This article is licensed under a Creative Commons Attribution 3.0 Unported Licence.

particles inside the sampling system was performed. Furthermore, a cleaning of the impactor of the SMPS in an ultrasonic bath enabled the same for this element before the first run and after the change from diesel to OME. After the fuel change, the engine ran several test cycles to remove remaining diesel residues in the fuel system or adhering soot in the engine or exhaust system. During this cleaning process, the sampling system ran with two-stage dilution and the CS with a set temperature of 350 °C and operated auxiliary pump.

Since the test runs could not take place on the same day under identical ambient conditions, a monitoring of the air temperature, ambient pressure, and humidity enabled an assumption regarding the comparability of the volatile particle measurement results. Nevertheless, the respective test runs with and without the CS happened on the same day, while the change of the fuel or the sampling position prevented a same-day-measurement. However, the ambient conditions for the test runs without removal of volatile particles differ by 1 °C in ambient temperature, 5% in humidity, and 6 mbar in ambient pressure. Three measurement recordings mapped the PSD in the exhaust gas at every stationary operation point.

For the tailpipe PN measurement of OME operation during the WHSC and WHTC based on the regulation No. 49 of the UN/ECE,[61] the chronological order of the test runs was as follows. Before every test cycle, the engine was pre-conditioned to the respective operating point of the WHSC according to the regulation. This study does not consider cold start operation in WHTC. This is due to the modular aftertreatment system, which has a poorer thermal behavior than a state-of-the art system. The first run consisted of a WHSC without DPF but with urea dosing, followed by WHTC with the same setup. Since the DPF was able to build up a soot layer in diesel operation, a regeneration of the DPF in an oven at 500 °C for six hours took place before reinstallation of the DPF in the ATS. The experiment continued with a run of a WHSC with DPF and urea dosing, followed by a run without urea dosing. Between these two runs, the engine ran in a regeneration mode without dosing, providing a cleaning of the SCR catalysts. A WHTC followed with the same order, beginning with urea dosing.

Results and discussion

The following chapter compares the PSD of diesel and OME at two engine operation points with different sampling points and different sampling systems. In order to compare the respective size distributions, the scale of the figures is the same in diesel and OME operation. The figures plot the data using normalized concentration according to the following formula:

$$\frac{\mathrm{d}N}{\mathrm{d}\log_{10} D_p} = \frac{\mathrm{d}N}{\log_{10} D_{\mathrm{p,u}} - \log_{10} D_{\mathrm{p,l}}} \quad (1)$$

dN describes the number of particles in the total concentration and $D_{\mathrm{p,u}}$ and $D_{\mathrm{p,l}}$ are the upper and lower bin boundaries, respectively. Therefore, the particle concentration is divided by the bin width. This gives a normalization which is independent of the specific bin width. This normalization enables comparison of particle concentrations between different measurement devices with different resolutions. The figures contain the average (arithmetic mean, abbreviated as avg) of three samples and the respective standard deviation (std). The average was filtered using a Savitzky–Golay filter of polynomial order 3 and frame length 21.

Fig. 3 shows the raw exhaust PSD for diesel and OME operation at the load points L1 and L2 without the catalytic stripper. Therefore, the PSD contains both volatile and solid particles.

The PSD in diesel operation showed a clear nucleation mode around 10 nm for both points, which originates mainly from volatile organic and sulfur compounds.[18] This mode also appeared in OME operation, with a similar level at L2 and with lower amplitude at L1. For both fuels, a significant part of the nucleation mode might be derived from the lube oil, since several studies demonstrated sub-23 nm particles even during engine motoring.[62–65] Diesel operation shows a bimodal distribution similar to the results of Abdul-Khalek *et al.*,[66] with a separate accumulation mode that describes its maximum at 40 nm in the same order of magnitude as the nucleation mode at L2. According to the relevant literature, this mode contains predominantly solid soot particles.[18] This accumulation mode also appeared at L1, but to a lesser degree than the respective nucleation mode. The exhaust in OME operation showed no accumulation mode on the same scale as in diesel operation.

In order to distinguish between volatile and solid particles in the exhaust, Fig. 4 shows the raw exhaust PSD for diesel and OME operation with the CS.

In diesel operation, both operating points show a broad accumulation mode of solid particles that is assumed to consist of soot particles. In contrast to the presentation of Fig. 3, this

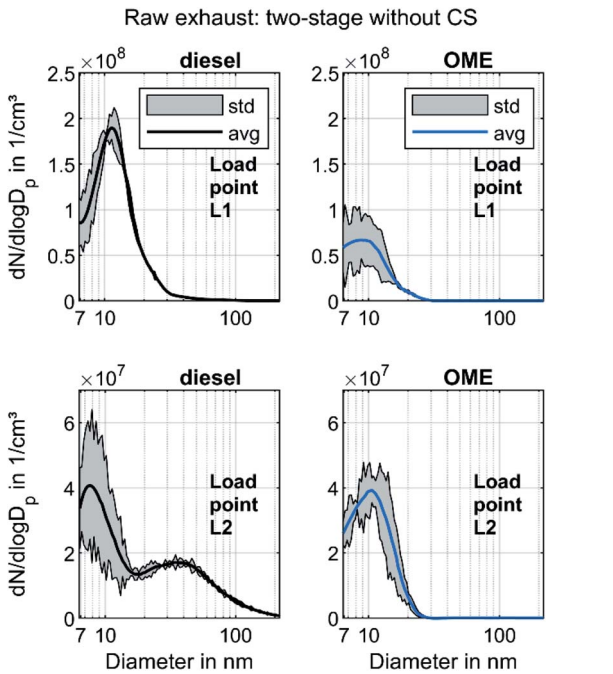

Fig. 3 Particle size distribution of OME and diesel raw exhaust without volatile particle remover and two-stage dilution: filtered average (arithmetic mean) of three recordings and indication of the standard deviation.

© 2022 The Author(s). Published by the Royal Society of Chemistry

Open Access Article. Published on 15 febbraio 2022. Downloaded on 01/08/2025 15:13:15.
This article is licensed under a Creative Commons Attribution 3.0 Unported Licence.

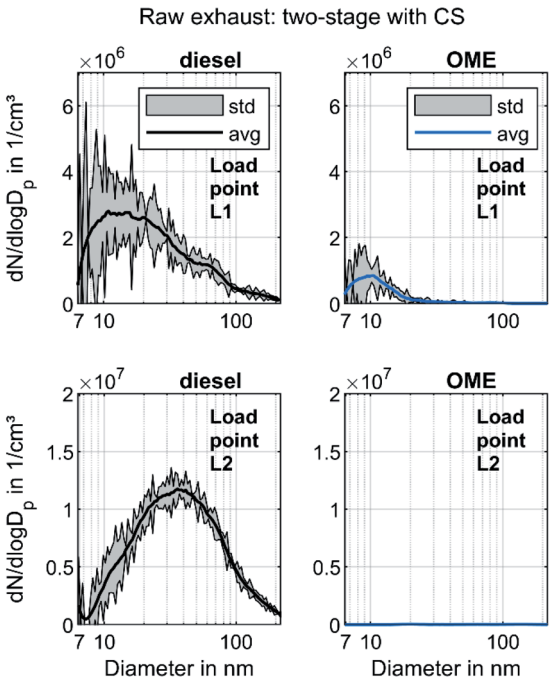

Fig. 4 Particle size distributions of OME and diesel raw exhaust with volatile particle remover and two-stage dilution: filtered average (arithmetic mean) of three recordings and indication of the standard deviation.

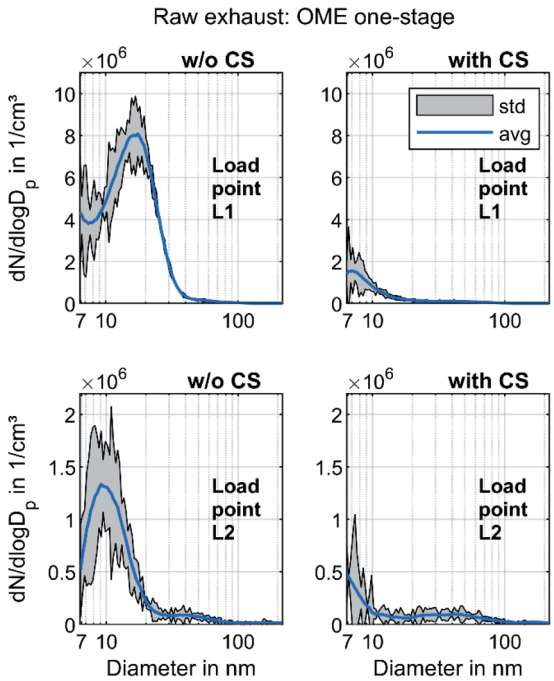

Fig. 5 Particle size distributions of OME raw exhaust with and without volatile particle remover and one-stage dilution: filtered average (arithmetic mean) of three recordings and indication of the standard deviation.

mode is clearly visible at L1, since the removal of the dominant mode of volatile particles by the CS enables the adjustment of the axis scale maximum to a lower value. At L2, the mode with a maximum at 40 nm remains unchanged and shows the same order of magnitude as without CS, which confirms the hypothesis that the observed mode in Fig. 3 consists of solid particles and builds the typical accumulation mode in diesel exhaust. In OME operation, the nucleation mode at L1 observed in Fig. 3 decreases in the same ratio as in diesel operation with usage of the CS. From this observation it follows that the majority of the nucleation mode around 10 nm is of a volatile nature. Since several studies confirm the soot-free combustion of OME, the remaining solid particles might consist mainly of engine oil ash or metallic abrasion.[18] At L2, no particle mode is visible with the same scaling of particulate emissions as in diesel operation. The comparison of the two fuels regarding solid particle size distributions shows lower particulate emission in OME operation, irrespective of the particle size range.

In order to investigate the size distribution in OME operation in more detail, the measurements are carried out with a one-stage dilution system as well. Fig. 5 depicts the PSD of OME using this sampling system with and without CS for the two operating points.

Without CS, the exhaust contained a strong nucleation mode similar to that observed in Fig. 3 at both operating points. While the maximum of this mode was at 10 nm at L2, the maximum moved in the direction of a larger diameter at L1. This might have been due to an increase in the particle growth rate due to the lower dilution ratio and subsequent cooling upstream of the SMPS.[67,68] With CS, the nucleation mode decreased, corresponding well to Fig. 4. The maximum was at less than 10 nm, in contrast to the curve without CS. This led to the assumption that these nonvolatile particle cores consisting of ash or metallic abrasion[29] form a shell with condensed hydrocarbons during cooling, leading to particle growth. Rönkkö *et al.* discovered this phenomenon in the exhaust of a heavy-duty diesel engine.[69] Furthermore, the nucleation mode observed without CS may have also contained condensed water droplets, since the concentration of water in the exhaust in OME operation was higher than 10% for the operating points investigated. Another possibility is the binary homogeneous nucleation of sulfuric acid and water.[70] Since OME is assumed to have a sulfur content of less than 1 ppm, this phenomenon is limited to sulfur originating from the engine oil, but it might still be present.[71] The PSD of Fig. 5 with CS did not contain these particle cores consisting of sulfuric acid, as sulfur is adsorbed in the Catalytic Stripper. Given the lower dilution ratio than in Fig. 5, an accumulation mode became visible at L2. This mode may consist of a small amount of soot particles. However, the observations in Fig. 5 refute the assumption of Barro *et al.*,[29] *i.e.*, that the particles forming the nucleation mode in OME exhaust are mostly of a solid nature. Based on the observations in Fig. 3–5, the authors propose that, in the case of a comparison with pollutant emission legislation such as Euro VI or upcoming regulations, the volatile fraction in OME exhaust must be removed, as it is the case for diesel exhaust according to the PMP.[21] The effect of an evaporation tube on OME exhaust will have to be studied in further investigations.

Open Access Article. Published on 15 febbraio 2022. Downloaded on 01/08/2025 15:13:15.
This article is licensed under a Creative Commons Attribution 3.0 Unported Licence.

Modern commercial heavy-duty engines that comply with today's emissions legislation, *e.g.* Euro VI, are equipped with a complex exhaust gas aftertreatment system. This system usually contains a diesel oxidation catalyst, a system for selective catalytic reduction and a diesel particulate filter. In order to evaluate the effectivity of these components regarding the particle removal efficiency, Fig. 6 presents the PSD at the tailpipe sampling point. The filtration efficiency (FE) was calculated according to the following formula and the values depicted in Fig. 4 and 5 were used:

$$\mathrm{FE} = \frac{\mathrm{PN_{raw}} - \mathrm{PN_{tailpipe}}}{\mathrm{PN_{raw}}} \quad (2)$$

The particle concentration at the tailpipe sampling position was near the detection limit of the SMPS, since it was in the range of 1–5 particles per cm^3 in every step interval of the classifier at both operating points. No clear difference between the PSD with and w/o CS was visible, so the volatile material that was detected in Fig. 5 might be oxidized in the aftertreatment system, predominantly in the DOC, as observed by Gren *et al.*[65] The particle concentrations at load point L2 were lower than those at L1. Rothe *et al.* discovered that some ash particles can penetrate the DPF at elevated temperatures.[72] Since L1 had higher exhaust gas temperatures than L2, this might be one reason. In addition, the friction between the piston and the liner is higher at L1 due to a higher load, with an associated higher piston side force and the lower engine speed resulting in higher proportions of solid and mixed friction.[73] Therefore, metallic abrasion might have been another reason for the higher particle concentrations at L1. Nevertheless, the FE curves in Fig. 6 confirmed that the aftertreatment system also ensured a reduction in solid particles even with a nearly empty DPF, which is assumed not to build up a soot layer in OME operation. This observation refutes the assumption by Omari *et al.*[27] They assumed that OME exhaust might become challenging for conventional particulate filters. The well-known filtration gap around 100 nm, which marks the transition between diffusive and impactive deposition,[54] also appeared in OME operation. Moreover, the results showed that the tailpipe level of total PN emissions in OME operation was significantly lower than the level in the raw exhaust, irrespective of sampling conditions.

Fig. 7 depicts the results of the investigation on the effect of urea dosing on nanoparticle emission. During the operation with urea dosing, both dosers provided AdBlue for SCR, with a reduction target of 100% for the nitrogen oxide emissions.

The operating points with active urea dosing formed a distinct nucleation mode. The particles survive the CS, which indicates that they were non-volatile. Several studies have observed increasing particle number emissions due to pure ammonia or urea solution dosing.[74,75] Mamakos *et al.* observed a formation of non-volatile particles due to urea injection, which spans from less than 10 nm to above 200 nm but with mode peaks below 20 nm.[76] Amanatidis *et al.* suggested that these particles consist of ammonium sulphate and ammonium bisulphate particles.[77] Since they observed the particle emissions even with pure ammonia, they ruled out impurities in the urea solution as the main reason. Schaber *et al.* observed the

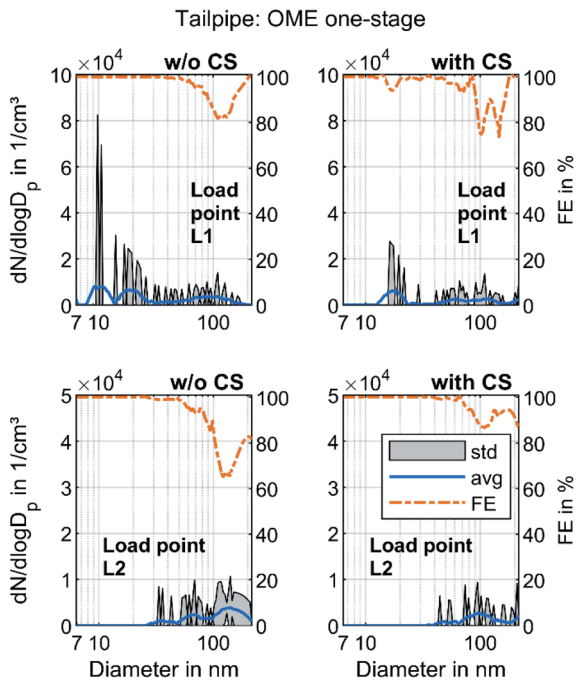

Fig. 6 Filtration efficiency FE of the aftertreatment system and particle size distributions of OME tailpipe exhaust with and without volatile particle remover and one-stage dilution: filtered average (arithmetic mean) of three recordings and indication of the standard deviation.

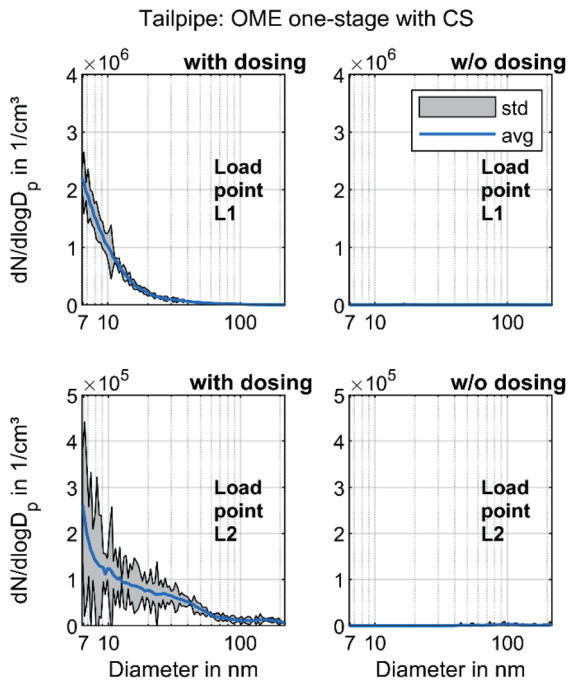

Fig. 7 Particle size distribution of OME tailpipe exhaust with and without urea dosing and one-stage dilution with volatile particle remover: filtered average (arithmetic mean) of three recordings and indication of the standard deviation.

© 2022 The Author(s). Published by the Royal Society of Chemistry

Open Access Article. Published on 15 febbraio 2022. Downloaded on 01/08/2025 15:13:15.
This article is licensed under a Creative Commons Attribution 3.0 Unported Licence.

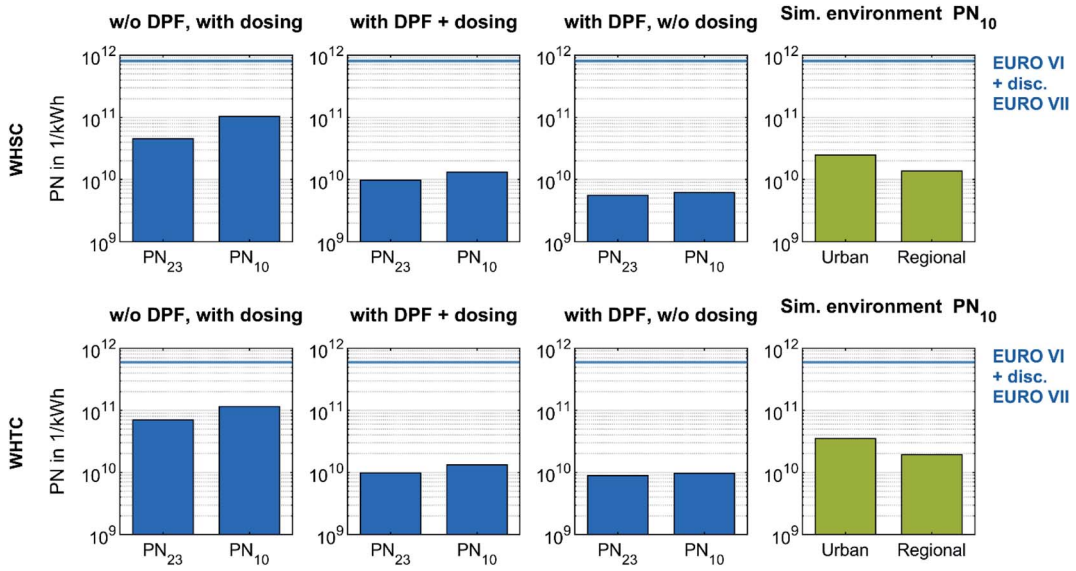

Fig. 8 Effect of DPF and urea dosing on particle number emissions during a stationary and transient test cycle fueled with OME. All test cycles result in PN emissions below the Euro VI legislation limit and furthermore below the discussed limit for Euro VII with a switch of the CPC setup towards a 50% cut-off at 10 nm. The simulated background evaluations of the test cycles use particle concentrations of Sun *et al.*,[80] who measured environmental particle concentrations from 10 to 800 nm Germany-wide.

formation of ammelides, ammelines and melamines *via* pyrolysis of urea in an open reaction vessel.[78] Börnhorst & Deutschmann attribute the formation of solid urea deposits to incomplete spray evaporation.[79] Regardless of what the solid particles are made of, Fig. 7 clarifies that they originated from the urea dosage and not from OME combustion. However, further research regarding their formation mechanisms and impact on human health and environment will be necessary.

Pre-conditioned WHSC and WHTC runs enabled an evaluation of the efficiency of the DPF in OME operation and the impact of urea dosing on particle number emission under stationary and transient driving conditions. The investigation on solid particle number (PN) emission in these test cycles used the PMP-conformant PN measurement system. In order to compare the PN emission with the Euro VII regulations discussed and in consideration of sub-23 nm particles,[19,20] a CPC with a 50% cut-off at 10 nm complemented the system. Fig. 8 depicts the PN emissions of the test cycles with different configurations on a logarithmic scale. PN_{23} describes the emission determined by the CPC inside the AVL APC 489, and PN_{10} describes the emission determined by the additional CPC.

In every configuration, the value of PN_{10} was higher than that of PN_{23}. Therefore, the solid particles in the form of ash originating from engine lube oil or in form of metallic abrasion originating from engine wear observed in Fig. 5 contributed more to the value of PN_{10} than to PN_{23}. The effect of the DPF is clear: the difference between PN_{10} and PN_{23} decreased during WHSC and WHTC, while the overall level of PN emission decreased as well. The filtration efficiency was similar to that shown in Fig. 6, confirming that the DPF was able to significantly reduce particle emissions in OME operation, regardless of whether the scope is for PN_{23} or PN_{10}. The PN increase due to urea dosing appears again in Fig. 8 comparison. In both test cycles, the reduction factor of PN by DPF was higher than the impact of urea dosing. Since the observed nucleation modes of urea-originated particles have their maxima below 10 nm in Fig. 7, this source of PN emissions may have been underestimated in Fig. 8. However, the PN emissions in the stationary and transient test cycle in OME operation were far below the limit values of Euro VI and the Euro VII values discussed, even without DPF and with urea dosing.

The bars on the right side of Fig. 8 represent the simulated cycle evaluation using the particle concentration of representative urban and regional backgrounds in Germany. These values of 6381 1 cm^{-3} and 3519 1 cm^{-3}, respectively, were derived from an estimation using the arithmetic mean of the medians of the measurements of Sun *et al.*,[80] who considered solid nanoparticles from 10 to 800 nm Germany-wide in 2018. This comparison demonstrates the ultra-low level of PN emissions of an OME heavy-duty engine equipped with an exhaust aftertreatment system. Nevertheless, the particles in the OME exhaust are assumed to consist of ash, metallic abrasion and soot, so their impact on human health and environment might be more serious than the urban background level.

Conclusions and outlook

The present work contains a comparison of particle size distributions in the raw exhaust of a heavy-duty engine in diesel and OME operations at two stationary operating points. Two sampling systems with a two-stage dilution were used in order to distinguish between PSD containing volatile material and PSD after removing volatile material *via* a catalytic stripper in general accordance with PMP specifications. In order to investigate the PSD in OME operation, a second dilution stage was removed in additional measurements. With this sampling

Open Access Article. Published on 15 febbraio 2022. Downloaded on 01/08/2025 15:13:15.
This article is licensed under a Creative Commons Attribution 3.0 Unported Licence.

system, the comparison between raw exhaust and tailpipe sampling showed the particle reduction efficiency of a modern aftertreatment system, containing oxidizing catalysts, a twin-dosing SCR system and a DPF. The effect of urea dosing on the PSD was investigated at the tailpipe sampling position. Test runs of the regulated test cycles WHSC and WHTC with and without DPF and with and without urea dosing demonstrated the ultra-low level of PN emissions in OME operation.

The results are summed up by the following conclusions:

The nucleation mode with a maximum at 10 nm in OME raw exhaust mainly consisted of volatile material. This is in contrast to assumptions made in previous studies.[27,29]

Because of the mostly soot-free combustion, OME exhaust shows smaller solid PN emissions than diesel, even in the sub-23 nm range. In this range, the solid particles are assumed to mainly consist of ash from engine lube oil and metallic abrasion. However, it cannot be ruled out that small soot particles also occur, because Barro *et al.* observed them in OME exhaust using TEM.[29]

The aftertreatment system reduced the particle concentration in OME exhaust. No difference between the PSD with and without removing volatile particles was visible at the tailpipe sampling position. The observed volatile material in the raw exhaust was therefore oxidized in the DOC and ASC.

An uncoated DPF showed a significant filtration efficiency in OME operation, in contrast to the assumption by Omari *et al.*[27]

Even given PN10 legislation with the current limit values, the OME still falls below the limits whether in stationary or transient operation, with and without DPF. However, the direct comparison with the limit value is only valid for the WHSC because this study used a pre-conditioned WHTC without cold start operation.

During these test cycles, the particle concentration in OME exhaust was lower than the concentration in a representative background of urban and regional areas in Germany. Nevertheless, the environmental impact of particles from OME exhaust is not clear.

Urea dosing leads to an increase of solid PN emissions, especially in the sub-23 nm range. Therefore, improvement of the SCR system is a target-oriented way of reducing PN emissions in an OME engine.

The conclusions are based on the observations in this study and are therefore limited to the methodology used.

Nevertheless, the following research will be necessary in the future:

The necessity of regenerating a DPF in OME combustion must be investigated. Similar effects to those observed by Rothe *et al.*[72] and Dimopoulos Eggenschwiler *et al.*[81] may occur, since they observed that the soot oxidation velocity decreases with a higher proportion of organic material on the particle surface.

Furthermore, an open channel filter may be a good approach for OME engines, since this offers a compromise between filtration efficiency and exhaust backpressure, leading to higher thermodynamic efficiency.[82]

A validation of the observed behavior using different sampling systems will be necessary. For example, Su *et al.* demonstrated a difference of on average 20% using a catalytic stripper and a dilution tunnel with an evaporation tube.[83]

In the context of future exhaust gas legislation, the impact of cold start operation on pollutant emissions may increase in importance. Therefore, further investigation in this area is essential.

In order to evaluate the sooting tendency of OME regardless of the parameters effecting soot formation in an engine, *e.g.* injection, exhaust gas recirculation and oxygen availability, investigations using a laminar burner as in Palazzo *et al.*[84] or McEnally *et al.*[85] will be necessary.

Furthermore, Bartholet *et al.* demonstrated that different molecular structures of OME and derivatives affect the nanoparticle behavior during combustion in a laminar burner.[86] This must be investigated in the inner-engine combustion environment.

Definitions and abbreviations

ASC	Ammonia slip catalyst
ATS	Aftertreatment system
avg	Average (arithmetic mean)
BHT	Butylated hydroxytoluene
CPC	Condensation particle counter
CS	Catalytic stripper CS10
DIL	Dilution
DOC	Diesel oxidation catalyst
$D_{p,l}$	Lower bin boundary
$D_{p,u}$	Upper bin boundary
dN	Number of particles
DPF	Diesel particulate filter
EGR	Exhaust gas recirculation
ET	Evaporation tube
FAME	Fatty acid methyl esters
FE	Filtration efficiency
HC	Hydrocarbon
HVO	Hydrogenated vegetable oil
Hyd	Hydrolysis catalyst
LHV	Lower heating value
MFB50	50% mass fraction burnt
OFA	Open frontal area
OME	Polyoxymethylene dimethyl ethers (with the specific mixture fractions used in this study)
$OME_{(n)}$	Polyoxymethylene dimethyl ethers (of the chain-length n)
PCRF	Particle concentration reduction factor
PGM	Platinum group metals
PMP	Particle measurement programme
PN	Particle number
PN_{23}	Particle number emission, determined *via* CPC with a 50% cut-off at 23 nm
PN_{10}	Particle number emission, determined *via* CPC with a 50% cut-off at 10 nm
PN_{raw}	Particle number, determined at raw exhaust sampling position
$PN_{tailpipe}$	Particle number, determined at tailpipe exhaust sampling position

© 2022 The Author(s). Published by the Royal Society of Chemistry

PSD	Particle size distribution
SCR	Selective catalytic reduction
SLPM	Standard liter per minute
SMPS	Scanning mobility particle sizer
std	Standard deviation
TDC	Top dead center
TEM	Transmission electron microscopy
UDP	Universal decomposition pipe
VPR	Volatile particle remover
WHSC	World harmonised steady-state cycle
WHTC	World harmonised transient cycle
λ	Air–fuel ratio

Open Access Article. Published on 15 febbraio 2022. Downloaded on 01/08/2025 15:13:15.
This article is licensed under a Creative Commons Attribution 3.0 Unported Licence.

Author contributions

Alexander D. Gelner: conceptualization, data curation, formal analysis, investigation, methodology, project administration, software, validation, visualization, writing – original draft, writing – review & editing. Dieter Rothe: methodology, resources, supervision, validation, writing – original draft, writing – review & editing Carsten Kykal: methodology, validation, writing – review & editing. Martin Irwin: methodology, resources, validation, writing – original draft, writing – review & editing. Alessandro Sommer: conceptualization, validation, writing – review & editing. Christian Pastoetter: conceptualization, supervision, funding acquisition, project administration, writing – review & editing. Martin Härtl: funding acquisition, project administration, supervision, writing – review & editing. Malte Jaensch: writing – review & editing. Georg Wachtmeister: funding acquisition, project administration, supervision, writing – review & editing.

Conflicts of interest

The authors declare that they have no known competing financial interests or personal relationship that could have appeared to influence the work reports in this paper. The Catalytic Stripper was provided by Catalytic Instruments GmbH & Co. KG and their involvement with this study was on an advisory basis only and had no bearing on the outcomes achieved.

Acknowledgements

The project "Sub-Zero-Emissions Dieselmotor" (grant number AZ-1266-17) was funded by the Bavarian Research Foundation (BFS) and was carried out in collaboration with MAN Truck & Bus SE, VT Vitesco Technologies Emitec GmbH, Chair of Analytical Chemistry of TUM and ASG Analytik-Service AG. Their support is gratefully acknowledged. The authors also want to thank Catalytic Instruments GmbH & Co. KG for providing a Catalytic Stripper. Furthermore, the authors want to thank Mr Florian Lindner (MAN Truck & Bus SE) for his support in commissioning urea dosage and Mr Patrick Swarovsky (MAN Truck & Bus SE) for providing a 10 nm-CPC and consultation in this study.

References

1 *Climate Change 2014: Synthesis Report : [longer Report]*, ed. R. K. Pachauri and L. Meyer, Intergovernmental Panel on Climate Change, Geneva, Switzerland, 2015.
2 N. Gray, S. McDonagh, R. O'Shea, B. Smyth and J. D. Murphy, Decarbonising ships, planes and trucks: An analysis of suitable low-carbon fuels for the maritime, aviation and haulage sectors, *Advances in Applied Energy*, 2021, **1**, 100008.
3 S. Schemme, R. C. Samsun, R. Peters and D. Stolten, Power-to-fuel as a key to sustainable transport systems – An analysis of diesel fuels produced from CO_2 and renewable electricity, *Fuel*, 2017, **205**, 198–221.
4 J. Burger, M. Siegert, E. Ströfer and H. Hasse, Poly(oxymethylene) dimethyl ethers as components of tailored diesel fuel: Properties, synthesis and purification concepts, *Fuel*, 2010, **89**(11), 3315–3319.
5 M. Held, Y. Tönges, D. Pélerin, M. Härtl, G. Wachtmeister and J. Burger, On the energetic efficiency of producing polyoxymethylene dimethyl ethers from CO_2 using electrical energy, *Energy Environ. Sci.*, 2019, **12**(3), 1019–1034.
6 L. Pellegrini, M. Marchionna, R. Patrini, C. Beatrice, N. Del Giacomo and C. Guido, Combustion Behaviour and Emission Performance of Neat and Blended Polyoxymethylene Dimethyl Ethers in a Light-Duty Diesel Engine, in *SAE Technical Paper Series. SAE International400 Commonwealth Drive*, SAE Technical Paper Series, Warrendale, PA, United States, 2012.
7 L. Pellegrini, M. Marchionna, R. Patrini and S. Florio, Emission Performance of Neat and Blended Polyoxymethylene Dimethyl Ethers in an Old Light-Duty Diesel Car, in *SAE Technical Paper Series. SAE International400 Commonwealth Drive*, SAE Technical Paper Series, Warrendale, PA, United States, 2013.
8 M. Härtl, P. Seidenspinner, E. Jacob and G. Wachtmeister, Oxygenate screening on a heavy-duty diesel engine and emission characteristics of highly oxygenated oxymethylene ether fuel OME1, *Fuel*, 2015, **153**, 328–335.
9 S. E. Iannuzzi, C. Barro, K. Boulouchos and J. Burger, Combustion behavior and soot formation/oxidation of oxygenated fuels in a cylindrical constant volume chamber, *Fuel*, 2016, **167**, 49–59.
10 A. Damyanov, P. Hofmann, B. Geringer, N. Schwaiger, T. Pichler and M. Siebenhofer, Biogenous ethers: production and operation in a diesel engine, *Automot. Engine Technol.*, 2018, **3**(1–2), 69–82.
11 H. Ogawa, N. Miyamoto and M. Yagi, Chemical-Kinetic Analysis on PAH Formation Mechanisms of Oxygenated Fuels, in *SAE Technical Paper Series. SAE International400 Commonwealth Drive*, SAE Technical Paper Series, Warrendale, PA, United States, 2003.
12 D. Pélerin, K. Gaukel, M. Härtl, E. Jacob and G. Wachtmeister, Potentials to simplify the engine system using the alternative diesel fuels oxymethylene ether OME1 and OME3−6 on a heavy-duty engine, *Fuel*, 2020, **259**, 116231.

© 2022 The Author(s). Published by the Royal Society of Chemistry

Open Access Article. Published on 15 febbraio 2022. Downloaded on 01/08/2025 15:13:15.
This article is licensed under a Creative Commons Attribution 3.0 Unported Licence.

13 D. Pélerin, K. Gaukel, M. Härtl and G. Wachtmeister, Nitrogen Oxide Reduction Potentials Using Dimethyl Ether and Oxymethylene Ether in a Heavy-Duty Diesel Engine, in *SAE Technical Paper Series. SAE International400 Commonwealth Drive*, SAE Technical Paper Series, Warrendale, PA, United States, 2020.

14 B. Gaston, J. M. Drazen, J. Loscalzo and J. S. Stamler, The biology of nitrogen oxides in the airways, *Am. J. Respir. Crit. Care Med.*, 1994, **149**(2 Pt 1), 538–551.

15 C. J. L. Murray, A. Y. Aravkin, P. Zheng, C. Abbafati, K. M. Abbas, M. Abbasi-Kangevari, *et al.*, Global burden of 87 risk factors in 204 countries and territories, 1990–2019: a systematic analysis for the Global Burden of Disease Study 2019, *The Lancet*, 2020, **396**(10258), 1223–1249.

16 K. Li, L. Chen, S. J. White, K. Han, B. Lv, K. Bao, *et al.*, Effect of nitrogen oxides (NO and NO_2) and toluene on SO 2 photooxidation, nucleation and growth: A smog chamber study, *Atmos. Res.*, 2017, **192**, 38–47.

17 T. C. Bond, S. J. Doherty, D. W. Fahey, P. M. Forster, T. Berntsen, B. J. DeAngelo, *et al.*, Bounding the role of black carbon in the climate system: A scientific assessment, *J. Geophys. Res.: Atmos.*, 2013, **118**(11), 5380–5552.

18 D. B. Kittelson, Engines and nanoparticles, *J. Aerosol Sci.*, 1998, **29**(5–6), 575–588.

19 B. Giechaskiel, J. Vanhanen, M. Väkevä and G. Martini, Investigation of vehicle exhaust sub-23 nm particle emissions, *Aerosol Sci. Technol.*, 2017, **51**(5), 626–641.

20 B. Giechaskiel, T. Lähde and Y. Drossinos, Regulating particle number measurements from the tailpipe of light-duty vehicles: The next step?, *Environ. Res.*, 2019, **172**, 1–9.

21 J. Andersson, A. Mamakos and B. Giechaskiel. *Particle Measurement Programme (PMP) Heavy-Duty Inter-laboratory Correlation Exercise (ILCE_HD)*, Publications Office, Luxembourg, 2010, EUR (Luxembourg), vol. 24561.

22 Q. Lin, K. L. Tay, W. Yu, W. Yang and Z. Wang, Effects of polyoxymethylene dimethyl ether 3 (PODE3) addition and injection pressure on combustion performance and particle size distributions in a diesel engine, *Fuel*, 2021, **283**, 119347.

23 J. Liu, Z. Liu, L. Wang, P. Wang, P. Sun, H. Ma, *et al.*, Effects of PODE/diesel blends on particulate matter emission and particle oxidation characteristics of a common-rail diesel engine, *Fuel Process. Technol.*, 2021, **212**, 106634.

24 F. Ferraro, C. Russo, R. Schmitz, C. Hasse and M. Sirignano, Experimental and numerical study on the effect of oxymethylene ether-3 (OME3) on soot particle formation, *Fuel*, 2021, **286**, 119353.

25 T. Popp, R. Lechner, M. Becker, M. Hebauer, N. O'Connell and M. Brautsch, Potentials of OME/diesel blends for stationary power production – Improving emission characteristics of a diesel CHP unit, *Appl. Therm. Eng.*, 2019, **153**, 483–492.

26 G. Richter and H. Zellbeck, Oxymethylene Ethers as an Alternative for Passenger Car Diesel Engines, *MTZ Worldw.*, 2017, **78**(12), 60–67.

27 A. Omari, B. Heuser, S. Pischinger and C. Rüdinger, Potential of long-chain oxymethylene ether and oxymethylene ether-diesel blends for ultra-low emission engines, *Appl. Energy*, 2019, **239**, 1242–1249.

28 J. Preuß, K. Munch and I. Denbratt, Performance and emissions of renewable blends with OME3-5 and HVO in heavy duty and light duty compression ignition engines, *Fuel*, 2021, **303**, 121275.

29 C. Barro, M. Parravicini, K. Boulouchos and A. Liati, Neat polyoxymethylene dimethyl ether in a diesel engine; part 2: Exhaust emission analysis, *Fuel*, 2018, **234**, 1414–1421.

30 P. Dworschak, V. Berger, M. Härtl and G. Wachtmeister, Neat Oxymethylene Ethers: Combustion Performance and Emissions of OME 2 OME 3 OME 4 and OME 5 in a Single-Cylinder Diesel Engine, in *SAE Technical Paper Series. SAE International400 Commonwealth Drive*, SAE Technical Paper Series, Warrendale, PA, United States, 2020.

31 P. Dworschak, V. Berger, M. Härtl and G. Wachtmeister, Particle Size Distribution Measurements of Neat and Water-Emulsified Oxymethylene Ethers in a Heavy-Duty Diesel Engine, *SAE Int. J. Fuels Lubr.*, 2020, **13**(2), 187–203.

32 I. S. Abdul-Khalek and D. B. Kittelson, Real Time Measurement of Volatile and Solid Exhaust Particles Using a Catalytic Stripper, in *SAE Technical Paper Series. SAE International400 Commonwealth Drive*, SAE Technical Paper Series, Warrendale, PA, United States, 1995.

33 J. Swanson and D. Kittelson, Evaluation of thermal denuder and catalytic stripper methods for solid particle measurements, *J. Aerosol Sci.*, 2010, **41**(12), 1113–1122.

34 DIN/TS 51699, Fuels - polyoxymethylene dimethyl ether (OME): Draft German Standard.

35 *DIN EN 590:2017-10 - Automotive Fuels - Diesel: Requirements and Test Methods; EN 590*, Beuth Verlag GmbH, Berlin, 2017, 2013+A1.

36 L. Lautenschütz, D. Oestreich, P. Seidenspinner, U. Arnold, E. Dinjus and J. Sauer, Physico-chemical properties and fuel characteristics of oxymethylene dialkyl ethers, *Fuel*, 2016, **173**, 129–137.

37 S. K. Hoekman, A. Broch, C. Robbins, E. Ceniceros and M. Natarajan, Review of biodiesel composition, properties, and specifications, *Renewable Sustainable Energy Rev.*, 2012, **16**(1), 143–169.

38 C. Barro, M. Parravicini and K. Boulouchos, Neat polyoxymethylene dimethyl ether in a diesel engine; part 1: Detailed combustion analysis, *Fuel*, 2019, **256**, 115892.

39 *ISO 22241-1:2019 - Diesel engines - NOx reduction agent AUS 32: Part 1*, Quality requirements, 2019, (43.060.40 Fuel Systems) 2019-02.

40 S. D. Yim, S. J. Kim, J. H. Baik, I. Nam, Y. S. Mok, J.-H. Lee, *et al.*, Decomposition of Urea into NH_3 for the SCR Process, *Ind. Eng. Chem. Res.*, 2004, **43**(16), 4856–4863.

41 M. Koebel, M. Elsener and T. Marti, NO_x-Reduction in Diesel Exhaust Gas with Urea and Selective Catalytic Reduction, *Combust. Sci. Technol.*, 1996, **121**(1–6), 85–102.

42 K. Kamasamudram, C. Henry, N. Currier and A. Yezerets, N_2O Formation and Mitigation in Diesel Aftertreatment Systems, *SAE Int. J. Engines*, 2012, **5**(2), 688–698.

 © 2022 The Author(s). Published by the Royal Society of Chemistry

Open Access Article. Published on 15 febbraio 2022. Downloaded on 01/08/2025 15:13:15.
This article is licensed under a Creative Commons Attribution 3.0 Unported Licence.

43 L. Tigges, A. Wiedensohler, K. Weinhold, J. Gandhi and H.-J. Schmid, Bipolar charge distribution of a soft X-ray diffusion charger, *J. Aerosol Sci.*, 2015, **90**, 77–86.
44 T. J. Johnson, R. T. Nishida, X. Zhang, J. P. Symonds, J. S. Olfert and A. M. Boies, Generating an aerosol of homogeneous, non-spherical particles and measuring their bipolar charge distribution, *J. Aerosol Sci.*, 2021, **153**, 105705.
45 D. B. Kittelson, W. F. Watts, J. C. Savstrom and J. P. Johnson, Influence of a catalytic stripper on the response of real time aerosol instruments to diesel exhaust aerosol, *J. Aerosol Sci.*, 2005, **36**(9), 1089–1107.
46 I. A. Khalek, Sampling System for Solid and Volatile Exhaust Particle Size, Number, and Mass Emissions, in *SAE Technical Paper Series. SAE International400 Commonwealth Drive*, SAE Technical Paper Series, Warrendale, PA, United States, 2007.
47 J. Swanson, D. Kittelson, B. Giechaskiel, A. Bergmann and M. Twigg, A Miniature Catalytic Stripper for Particles Less Than 23 Nanometers, *SAE Int. J. Fuels Lubr.*, 2013, **6**(2), 542–551.
48 S. Amanatidis, L. Ntziachristos, B. Giechaskiel, D. Katsaounis, Z. Samaras and A. Bergmann, Evaluation of an oxidation catalyst ("catalytic stripper") in eliminating volatile material from combustion aerosol, *J. Aerosol Sci.*, 2013, **57**, 144–155.
49 L. Ntziachristos, S. Amanatidis, Z. Samaras, B. Giechaskiel and A. Bergmann, Use of a Catalytic Stripper as an Alternative to the Original PMP Measurement Protocol, *SAE Int. J. Fuels Lubr.*, 2013, **6**(2), 532–541.
50 Y. Otsuki, K. Takeda, K. Haruta and N. Mori, A Solid Particle Number Measurement System Including Nanoparticles Smaller than 23 Nanometers, in *SAE Technical Paper Series. SAE International400 Commonwealth Drive*, SAE Technical Paper Series, Warrendale, PA, United States, 2014.
51 S. Amanatidis, L. Ntziachristos, P. Karjalainen, E. Saukko, P. Simonen, N. Kuittinen, *et al.*, Comparative performance of a thermal denuder and a catalytic stripper in sampling laboratory and marine exhaust aerosols, *Aerosol Sci. Technol.*, 2018, **52**(4), 420–432.
52 B. Giechaskiel, A. D. Melas, T. Lähde and G. Martini, Non-Volatile Particle Number Emission Measurements with Catalytic Strippers: A Review, *Vehicles*, 2020, **2**(2), 342–364.
53 S.-L. von de Weiden, F. Drewnick and S. Borrmann, Particle Loss Calculator – a new software tool for the assessment of the performance of aerosol inlet systems, *Atmos. Meas. Tech.*, 2009, **2**(2), 479–494.
54 W. C. Hinds, *Aerosol Technology: Properties, Behavior, and Measurement of Airborne Particles*, Wiley, 1999.
55 P. Kulkarni, P. A. Baron and K. Willeke, *Aerosol Measurement*, John Wiley & Sons, Inc, Hoboken, NJ, USA, 2011.
56 L. Talbot, R. K. Cheng, R. W. Schefer and D. R. Willis, Thermophoresis of particles in a heated boundary layer, *J. Fluid Mech.*, 1980, **101**(4), 737–758.
57 B. Y. Liu, D. Y. Pui, K. L. Rubow and W. W. Szymanski, Electrostatic effects in aerosol sampling and filtration, *Ann. Occup. Hyg.*, 1985, **29**(2), 251–269.
58 C. S.-J. Tsai, Characterization of Airborne Nanoparticle Loss in Sampling Tubing, *J. Occup. Environ. Hyg.*, 2015, **12**(8), D161–D167.
59 C. Asbach, H. Kaminski, Y. Lamboy, U. Schneiderwind, M. Fierz and A. M. Todea, Silicone sampling tubes can cause drastic artifacts in measurements with aerosol instrumentation based on unipolar diffusion charging, *Aerosol Sci. Technol.*, 2016, **50**(12), 1375–1384.
60 B. Giechaskiel, L. Ntziachristos and Z. Samaras, Effect of ejector dilutors on measurements of automotive exhaust gas aerosol size distributions, *Meas. Sci. Technol.*, 2009, **20**(4), 45703.
61 Office P, *Regulation No 49 of the Economic Commission for Europe of the United Nations (UN/ECE) — Uniform Provisions Concerning the Measures to Be Taken against the Emission of Gaseous and Particulate Pollutants from Compression-Ignition Engines and Positive Ignition Engines for Use in Vehicles*, 2013.
62 T. Rönkkö, L. Pirjola, L. Ntziachristos, J. Heikkilä, P. Karjalainen, R. Hillamo, *et al.*, Vehicle engines produce exhaust nanoparticles even when not fueled, *Environ. Sci. Technol.*, 2014, **48**(3), 2043–2050.
63 P. Karjalainen, L. Ntziachristos, T. Murtonen, H. Wihersaari, P. Simonen, F. Mylläri, *et al.*, Heavy Duty Diesel Exhaust Particles during Engine Motoring Formed by Lube Oil Consumption, *Environ. Sci. Technol.*, 2016, **50**(22), 12504–12511.
64 S. Blochum, F. H. Ruch, T. Bastuck, M. Härtl, R. Mittler and G. Wachtmeister, Identification of In-Cylinder Aerosol Flow Induced Emissions due to Piston Ring Design in a DISI Single Cylinder LV Engine Using Oxygenated Synthetic Fuels, in *SAE Technical Paper Series. SAE International400 Commonwealth Drive*, SAE Technical Paper Series, Warrendale, PA, United States, 2021.
65 L. Gren, V. B. Malmborg, J. Falk, L. Markula, M. Novakovic, S. Shamun, *et al.*, Effects of renewable fuel and exhaust aftertreatment on primary and secondary emissions from a modern heavy-duty diesel engine, *J. Aerosol Sci.*, 2021, **156**, 105781.
66 I. S. Abdul-Khalek, D. B. Kittelson, B. R. Graskow, Q. Wei and F. Bear, Diesel Exhaust Particle Size: Measurement Issues and Trends, in *SAE Technical Paper Series. SAE International400 Commonwealth Drive*, SAE Technical Paper Series, Warrendale, PA, United States, 1998.
67 I. A. Khalek, D. B. Kittelson and F. Brear, Nanoparticle Growth During Dilution and Cooling of Diesel Exhaust: Experimental Investigation and Theoretical Assessment, in *SAE Technical Paper Series. SAE International400 Commonwealth Drive*, SAE Technical Paper Series, Warrendale, PA, United States, 2000.
68 U. Mathis, J. Ristimäki, M. Mohr, J. Keskinen, L. Ntziachristos, Z. Samaras, *et al.*, Sampling Conditions for the Measurement of Nucleation Mode Particles in the Exhaust of a Diesel Vehicle, *Aerosol Sci. Technol.*, 2004, **38**(12), 1149–1160.
69 T. Rönkkö, A. Virtanen, J. Kannosto, J. Keskinen, M. Lappi and L. Pirjola, Nucleation mode particles with

Open Access Article. Published on 15 febbraio 2022. Downloaded on 01/08/2025 15:13:15.
This article is licensed under a Creative Commons Attribution 3.0 Unported Licence.

a nonvolatile core in the exhaust of a heavy duty diesel vehicle, *Environ. Sci. Technol.*, 2007, **41**(18), 6384–6389.

70 J. I. Steinfeld, Atmospheric Chemistry and Physics: From Air Pollution to Climate Change, *Environment*, 1998, **40**(7), 26.

71 P. Karjalainen, T. Rönkkö, L. Pirjola, J. Heikkilä, M. Happonen, F. Arnold, *et al.*, Sulfur driven nucleation mode formation in diesel exhaust under transient driving conditions, *Environ. Sci. Technol.*, 2014, **48**(4), 2336–2343.

72 D. Rothe, M. Knauer, G. Emmerling, D. Deyerling and R. Niessner, Emissions during active regeneration of a diesel particulate filter on a heavy duty diesel engine: Stationary tests, *J. Aerosol Sci.*, 2015, **90**, 14–25.

73 A. Merkle, S. Kunkel and G. Wachtmeister, Analysis of the Mixed Friction in the Piston Assembly of a SI Engine, *SAE Int. J. Engines*, 2012, **5**(3), 1487–1497.

74 K. Arun Prasath, H. Bernemyr and A. Erlandsson, On the Effects of Urea and Water Injection on Particles across the SCR Catalyst in a Heavy - Duty Euro VI Diesel Engine, in *SAE Technical Paper Series. SAE International400 Commonwealth Drive*, SAE Technical Paper Series, Warrendale, PA, United States, 2020.

75 M. A. Robinson, J. Backhaus, R. Foley and Z. G. Liu, The Effect of Diesel Exhaust Fluid Dosing on Tailpipe Particle Number Emissions, in, *SAE Technical Paper Series. SAE International400 Commonwealth Drive*, SAE Technical Paper Series, Warrendale, PA, United States, 2016.

76 A. Mamakos, M. Schwelberger, M. Fierz and B. Giechaskiel, Effect of selective catalytic reduction on exhaust nonvolatile particle emissions of Euro VI heavy-duty compression ignition vehicles, *Aerosol Sci. Technol.*, 2019, **53**(8), 898–910.

77 S. Amanatidis, L. Ntziachristos, B. Giechaskiel, A. Bergmann and Z. Samaras, Impact of selective catalytic reduction on exhaust particle formation over excess ammonia events, *Environ. Sci. Technol.*, 2014, **48**(19), 11527–11534.

78 P. M. Schaber, J. Colson, S. Higgins, D. Thielen, B. Anspach and J. Brauer, Thermal decomposition (pyrolysis) of urea in an open reaction vessel, *Thermochim. Acta*, 2004, **424**(1–2), 131–142.

79 M. Börnhorst and O. Deutschmann, Advances and challenges of ammonia delivery by urea-water sprays in SCR systems, *Prog. Energy Combust. Sci.*, 2021, **87**, 100949.

80 J. Sun, W. Birmili, M. Hermann, T. Tuch, K. Weinhold, G. Spindler, *et al.*, Variability of black carbon mass concentrations, sub-micrometer particle number concentrations and size distributions: results of the German Ultrafine Aerosol Network ranging from city street to High Alpine locations, *Atmos. Environ.*, 2019, **202**, 256–268.

81 P. Dimopoulos Eggenschwiler and D. Schreiber, Investigation of the Oxidation Behavior of Soot in Diesel Particle Filter structures, in *SAE Technical Paper Series. SAE International400 Commonwealth Drive*, SAE Technical Paper Series, Warrendale, PA, United States, 2015.

82 J. Heikkilä, T. Rönkkö, T. Lähde, M. Lemmetty, A. Arffman, A. Virtanen, *et al.*, Effect of open channel filter on particle emissions of modern diesel engine, *J. Air Waste Manage. Assoc.*, 2009, **59**(10), 1148–1154.

83 S. Su, T. Lv, Y. Lai, J. Mu, Y. Ge and B. Giechaskiel, Particulate emissions of heavy duty diesel engines measured from the tailpipe and the dilution tunnel, *J. Aerosol Sci.*, 2021, **156**, 105799.

84 N. Palazzo, M. Kögl, P. Bauer, M. N. Mannazhi, L. Zigan, F. J. T. Huber, *et al.*, Investigation of Soot Formation in a Novel Diesel Fuel Burner, *Energies*, 2019, **12**(10), 1993.

85 C. Mcenally and L. Pfefferle, Improved sooting tendency measurements for aromatic hydrocarbons and their implications for naphthalene formation pathways, *Combust. Flame*, 2007, **148**(4), 210–222.

86 D. L. Bartholet, M. A. Arellano-Treviño, F. L. Chan, S. Lucas, J. Zhu, P. C. St. John, *et al.*, Property predictions demonstrate that structural diversity can improve the performance of polyoxymethylene ethers as potential bio-based diesel fuels, *Fuel*, 2021, **295**, 120509.

© 2022 The Author(s). Published by the Royal Society of Chemistry